Supplementary Information

Mass-encoded synthetic biomarkers for multiplexed urinary monitoring of disease

Gabriel A. Kwong[1,2], Geoffrey von Maltzahn[1,2,3], Gayathree Murugappan[1,4], Omar Abudayyeh[1], Steven Mo[1], Ioannis A. Papayannopoulos[2,5], Deanna Y. Sverdlov[6], Susan B. Liu[6], Andrew D. Warren[1,2], Yury Popov[6], Detlef Schuppan[6,7] & Sangeeta N. Bhatia[1,2,8,9,10]

[1] Harvard-MIT Health Sciences and Technology, Massachusetts Institute of Technology, Cambridge, MA, USA. [2] David H. Koch Institute for Integrative Cancer Research, Massachusetts Institute of Technology, Cambridge, MA, USA. [3] Current address: VentureLabs, The Flagship Innovation Factory, Cambridge, MA, USA. [4] Harvard Medical School, Boston, MA, USA. [5] Swanson Biotechnology Center, Massachusetts Institute of Technology, MA, USA. [6] Division of Gastroenterology and Hepatology, Beth Israel Deaconess Medical Center and Harvard Medical School, Boston, MA, USA. [7] Division of Molecular and Translational Medicine, Department of Medicine I, University of Mainz Medical School, Mainz, Germany. [8] Electrical Engineering and Computer Science, Massachusetts Institute of Technology, Cambridge, MA, USA. [9] Department of Medicine, Brigham and Women's Hospital and Harvard Medical School, Boston, MA, USA. [10] Howard Hughes Medical Institute, Chevy Chase, Maryland, USA.

Correspondence should be addressed to S.N.B. (sbhatia@mit.edu).

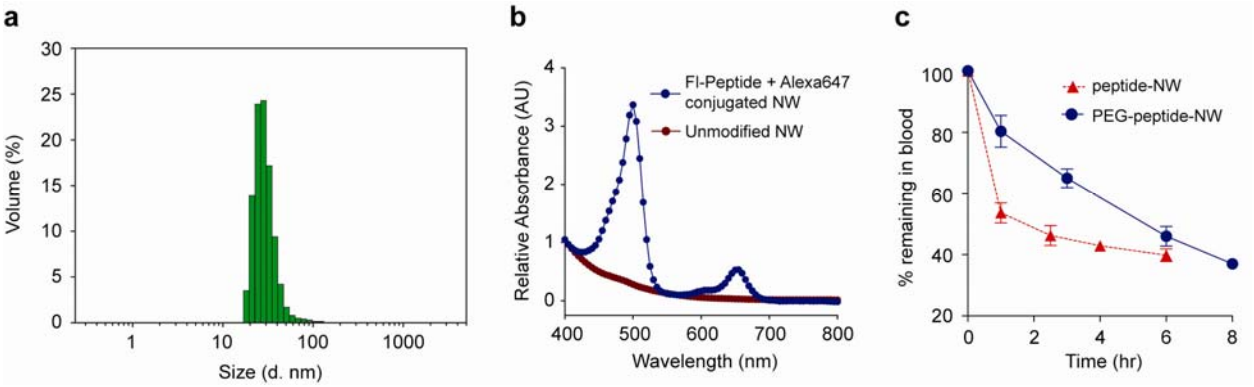

Supplementary Figure 1. Long-circulating iron oxide nanoworm chaperones. (**a**) Size distribution of dextran-coated, iron oxide NWs as determined by dynamic light scattering. (**b**) Absorbance spectra of free NWs (red) and NWs conjugated with Fluorescein-labeled peptides (~ 500 nm) and Alexa 647 (blue). (**c**) *In vivo* clearance kinetics of PEG-coated (blue) and PEG-free (red) NWs conjugated with substrate peptides. Pegylated NWs extended circulation half-life by ~4 hours.

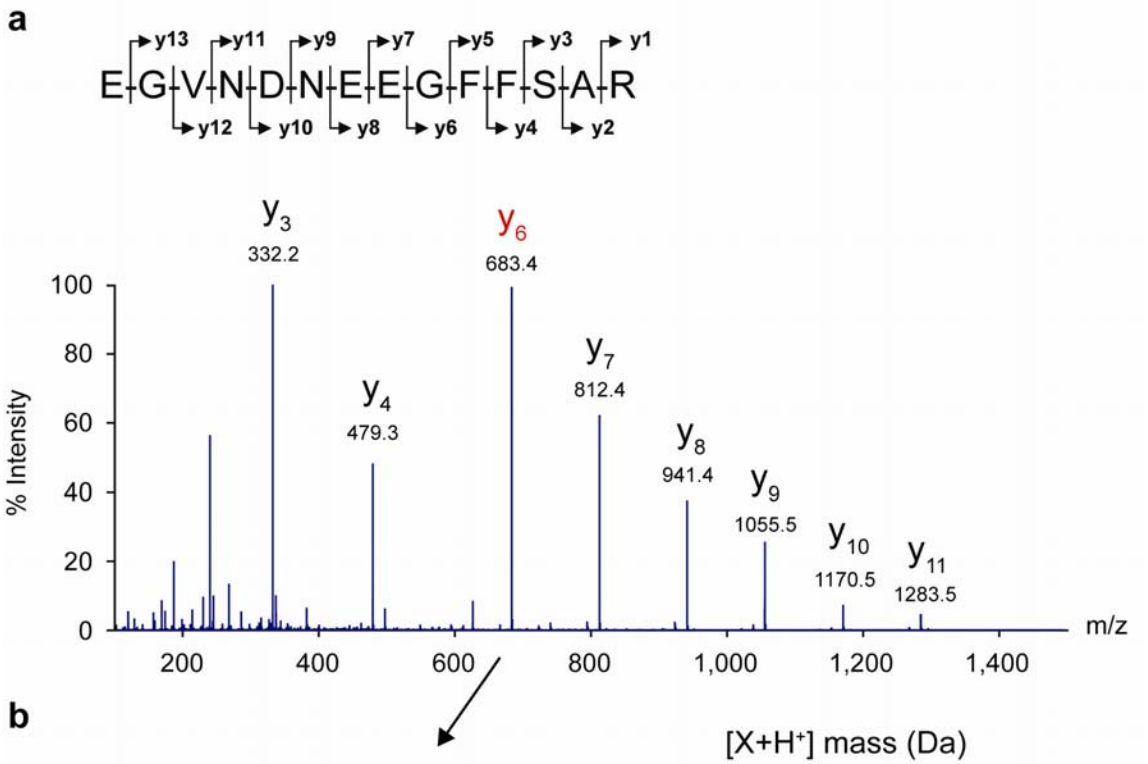

b

Balance Reporter (y_6 ion)	[X+H⁺] mass (Da) Balance	Reporter	Total
E^{+3}G^{+6}VNDNEE-GFFSAR	895.3	683.3	1578.7
E^{+2}G^{+6}VNDNEE-$^{+1}$GFFSAR	894.3	684.3	1578.7
E^{+1}G^{+6}VNDNEE-$^{+2}$GFFSAR	893.3	685.3	1578.7
EG^{+6}VNDNEE-$^{+2}$GFFS^{+1}AR	892.3	686.3	1578.7
EG^{+5}VNDNEE-GFFS^{+4}AR	891.3	687.3	1578.7
E^{+3}G^{+1}VNDNEE-$^{+1}$GFFS^{+4}AR	890.3	688.3	1578.7
E^{+3}GVNDNEE-G^{+6}FFSAR	889.3	689.3	1578.7
E^{+2}GVNDNEE-G^{+6}FFS^{+1}AR	888.3	690.3	1578.7
EG^{+1}VNDNEE-$^{+2}$G^{+6}FFSAR	887.3	691.3	1578.7
EGVNDNEE-$^{+3}$G^{+6}FFSAR	886.3	692.3	1578.7

Supplementary Figure 2. Isobaric COded REporter (iCORE) mass encoding. (**a**) MS/MS spectrum of Glu-fib following collision induced disassociation. Peaks correspond to c-terminal, y-type peptide fragments. (**b**) List of 10 isotopic analogs and corresponding masses produced via isobaric encoding. Each sequence was constructed by selectively enriching the balance or reporter regions with 'heavy' amino acids to produce unique y_6 reporter ions while maintaining a uniform total mass.

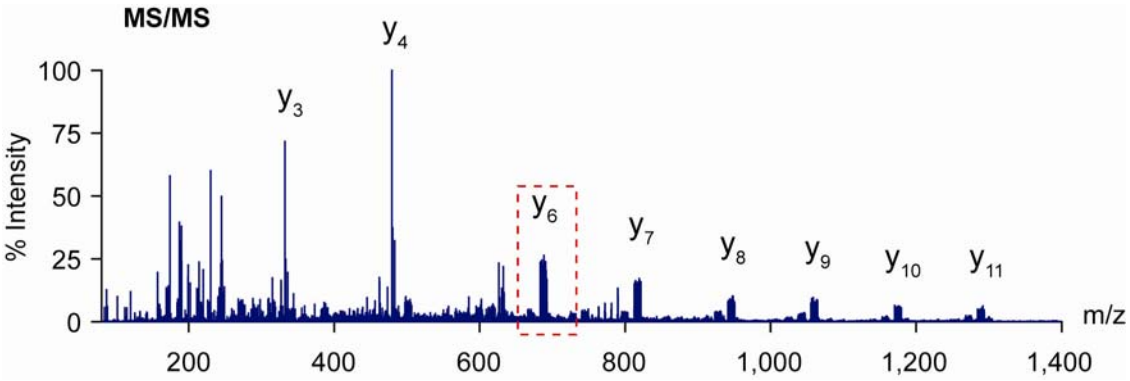

Supplementary Figure 3. MS/MS spectrum of 10-plex iCORE library. iCORE peak clusters centered on y-type ions. The y_6 region outlined by a red box is presented as **Figure 3e**.

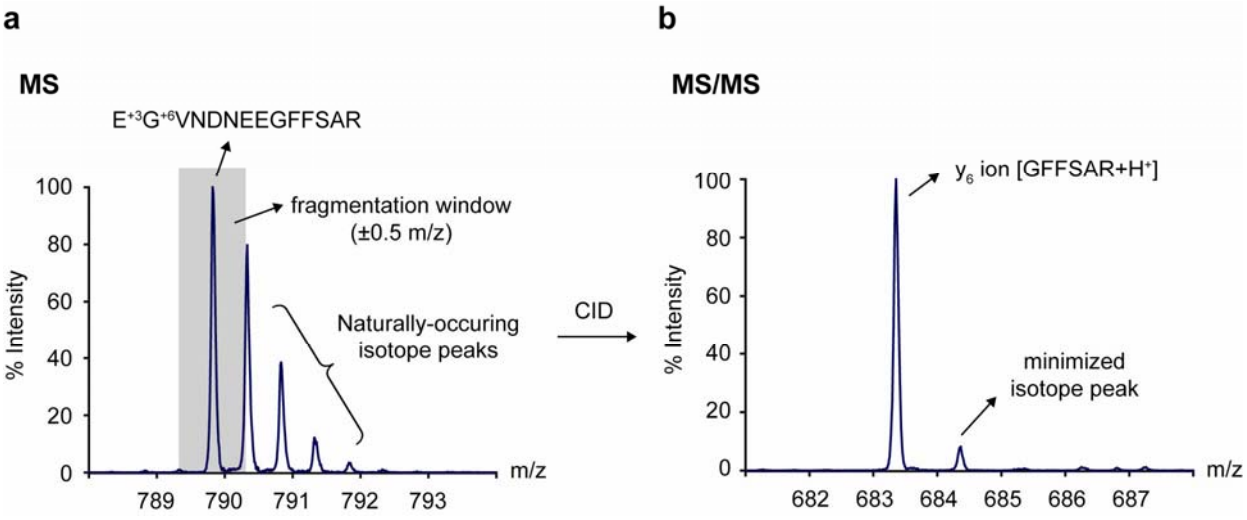

Supplementary Figure 4. Unit collection window for peptide fragmentation minimizes peak overlap arising from naturally occurring isotopes. (**a**) A typical MS spectrum of an isotope-coded Glu-fib peptide. The parent precursor peptide was collected for fragmentation via a unit mass window (gray), excluding the naturally occurring isotope peaks. (**b**) Resulting MS/MS spectrum. Isotope peak was minimized, comprising ~5% of the original peak intensity.

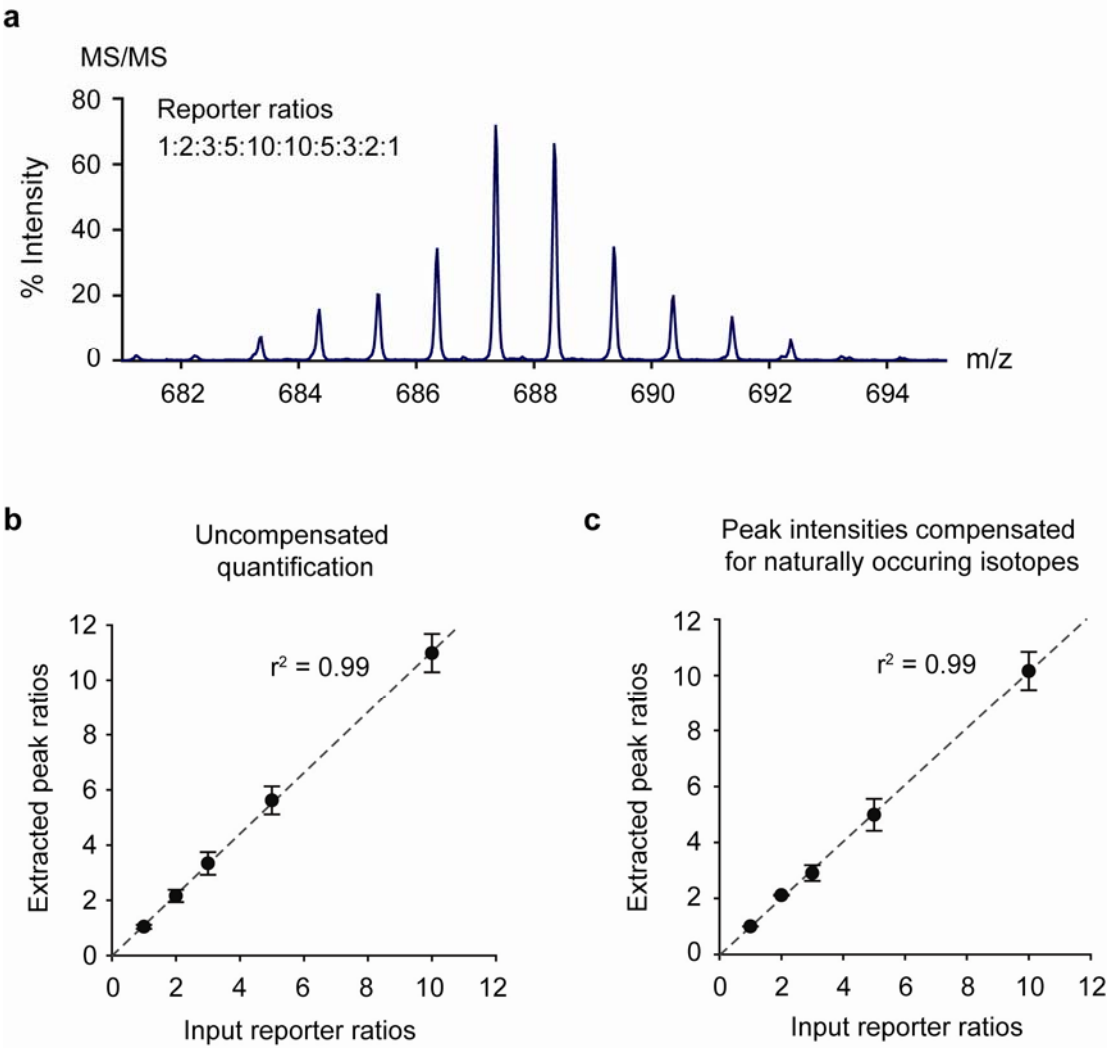

Supplementary Figure 5. iCORE LC MS/MS analysis is quantitative. (**a**) MS/MS spectrum of a 10-plex mixture of iCORE reporters combined in a 1:2:3:5:10:10:5:3:2:1 ratio. (**b**) Extracted peak intensities were highly correlated with the input reporter stoichiometry (r^2 = 0.99; n = 3; error bars = s.e.m.). (**c**) To account for naturally occurring isotopes (**Supplementary Fig. 4**), individual reporter intensities were modified by subtracting 5% of the prior reporter intensity. Compensated reporter ratios also strongly correlated with reporter ratios (r^2 = 0.99; n = 3; error bars = s.e.m.).

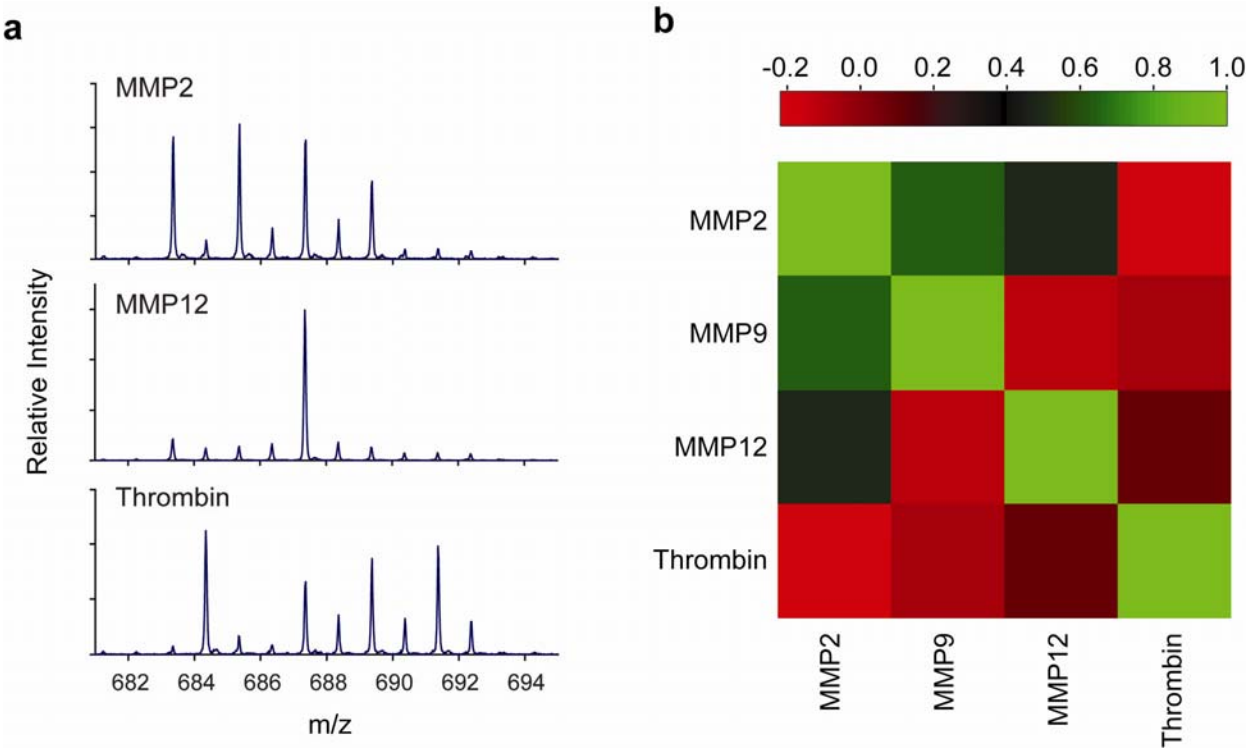

Supplementary Figure 6. Protease-specific iCORE mass signatures. (**a**) iCORE MS/MS profiles of recombinant proteases MMP2, MMP12, and thrombin. (**b**) Graphical representation of Pearson's correlation coefficients between proteases.

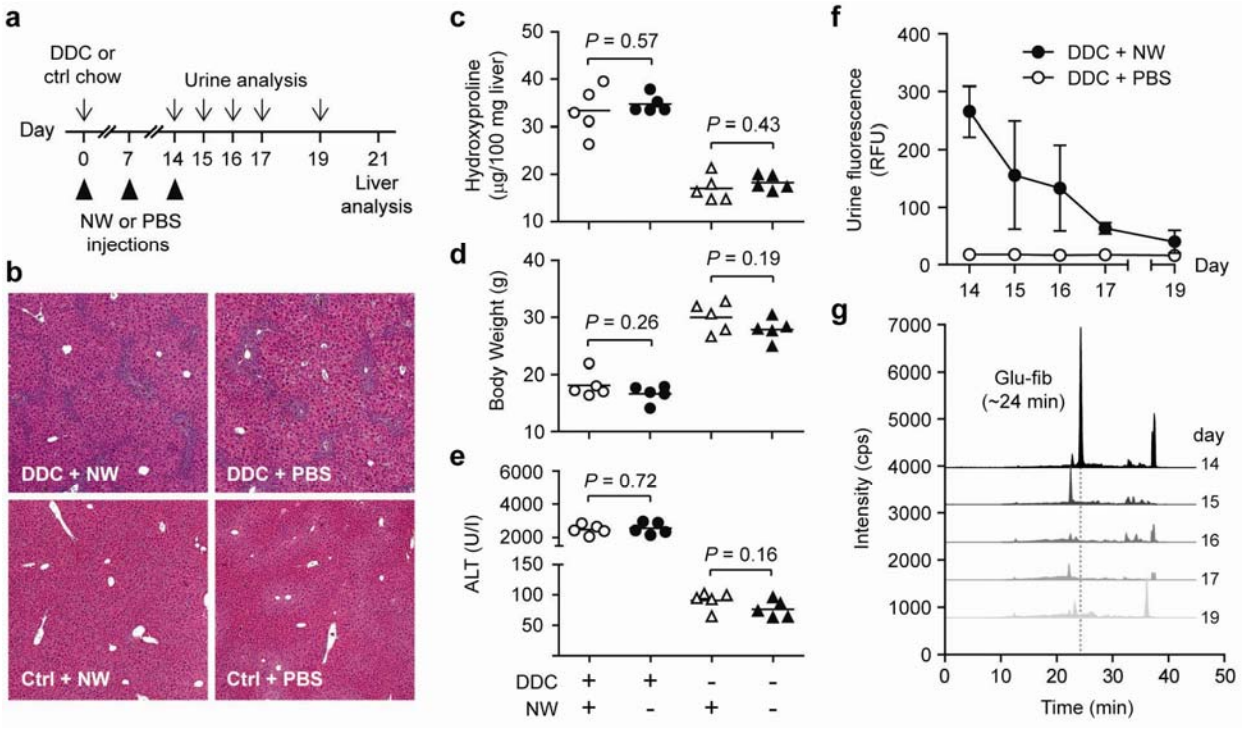

Supplementary Figure 7. Evaluation of NW toxicity and urinary clearance of reporters following repeated infusions. (**a**) Timeline of study. FVB/NJ mice fed DDC or control chow received weekly injections of NWs or PBS (triangle). Urine analysis was performed starting at day 14 (arrows) and livers were harvested and analyzed on day 21. (**b**) Histological sections of treatment groups showed no macroscopic alterations in fibrosis between NW and PBS treated animals. (**c**) Liver collagen by hydroxyproline analysis, (**d**) bodyweights, and (**e**) serum ALT levels were likewise unaltered (two-tailed T test). (**f**) Monitoring the decay of urinary fluorescence by FITC immunoprecipitation. By day 19, residual fluorescent reporters from the last NW injection (day 14), were no longer detectable (n = 5, s.d.). (**g**) Extracted ion chromatograms of mass 785.4 m/z from urine samples after day 14. No evidence of Glu-fib (peak elution time ~ 24 min.) was observed by day 15, one day after last NW infusion.

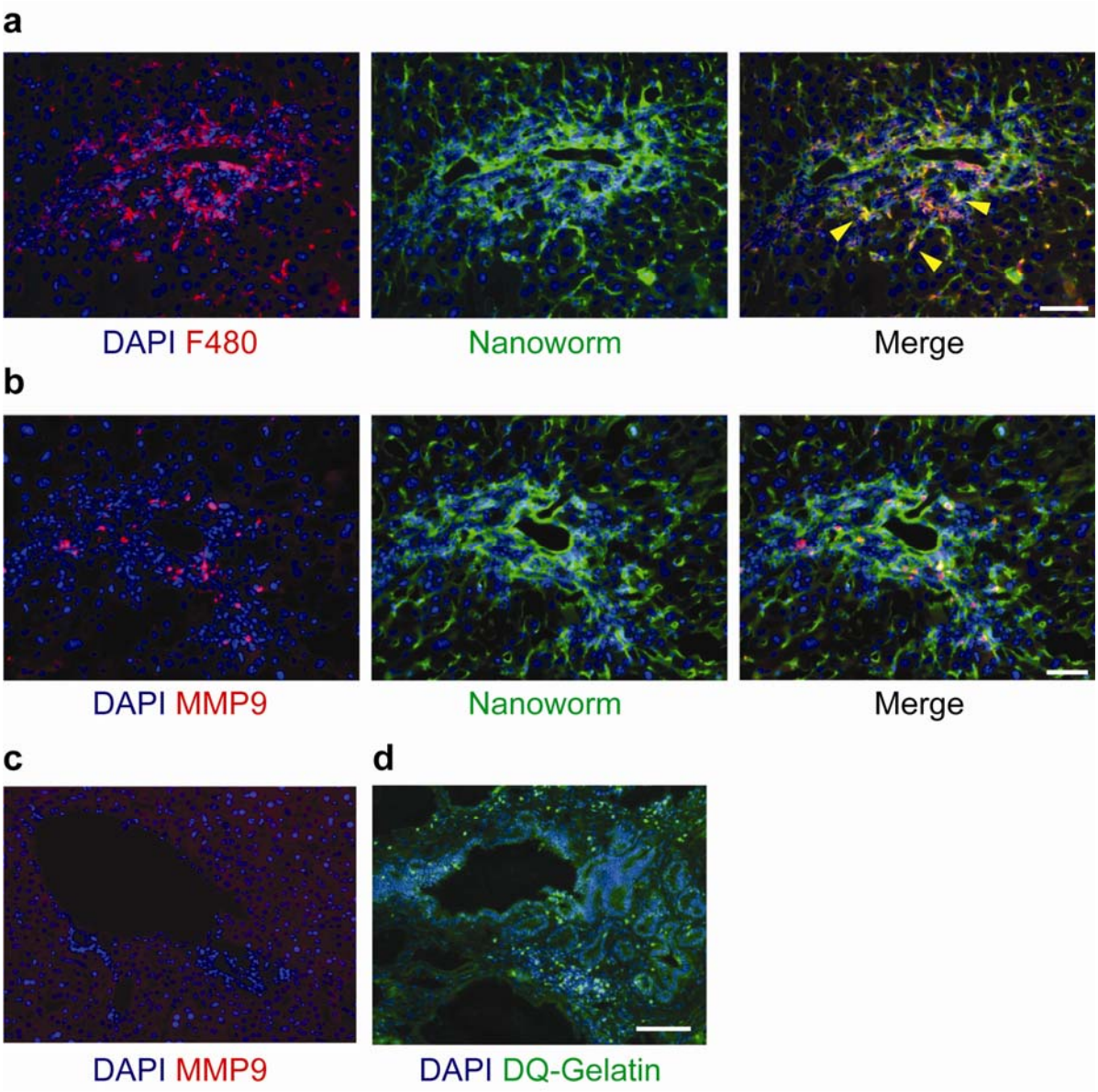

Supplementary Figure 8. Immunofluorescence of liver sections. (**a**) Periportal images of macrophage (red) and NW (green) infiltrate into fibrosing zones. Yellow arrows highlight areas of colocalization. (**b**) Periportal images of MMP9 (red) and NW (green). (**c**) MMP9 expression was not found in healthy livers. (**d**) Fluorescence image of periportal zone after gelatin *in situ* zymography. Scale bars = 100 μm.

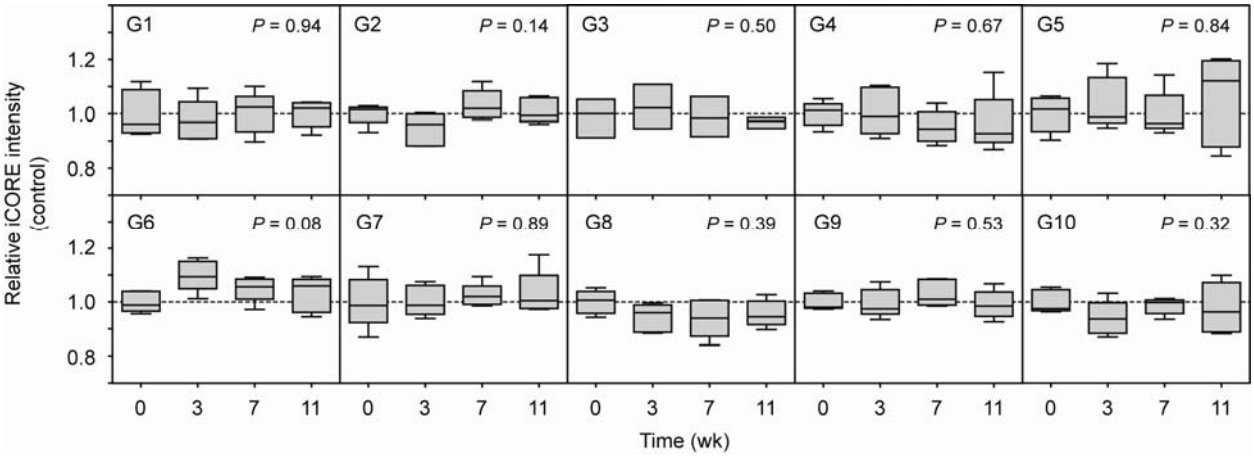

Supplementary Figure 9. iCORE profiles of control animals. Box-and-whisker plots of individual iCORE peak intensities (repeated measures ANOVA, n = 5).

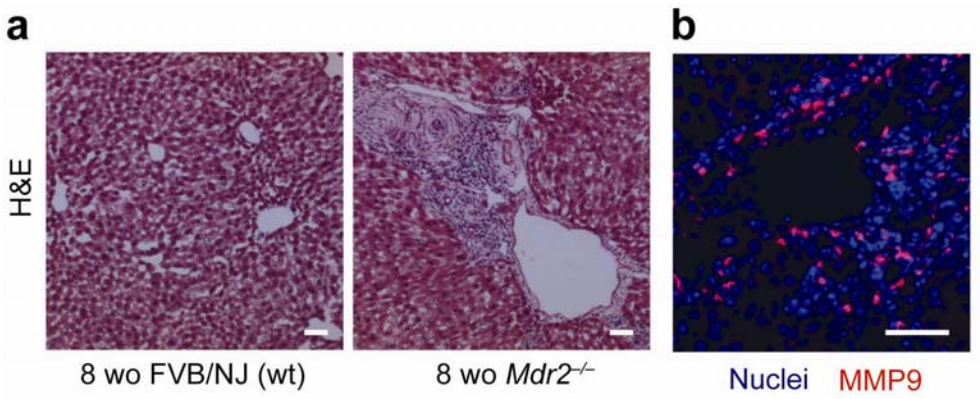

Supplementary Figure 10. *Mdr2*$^{-/-}$ mice spontaneously develop liver fibrosis from birth. (**a**) Histological staining of wild type FVB/NJ and *Mdr2*$^{-/-}$ knockout mice at 8 weeks of age. Significant periportal fibrosis was observed in *Mdr2*$^{-/-}$ liver sections. (**b**) Immunofluorescence staining of MMP9. Significant upregulation of MMP9 was observed in knockout animals at 8 weeks of age (scale bars = 100 μm).

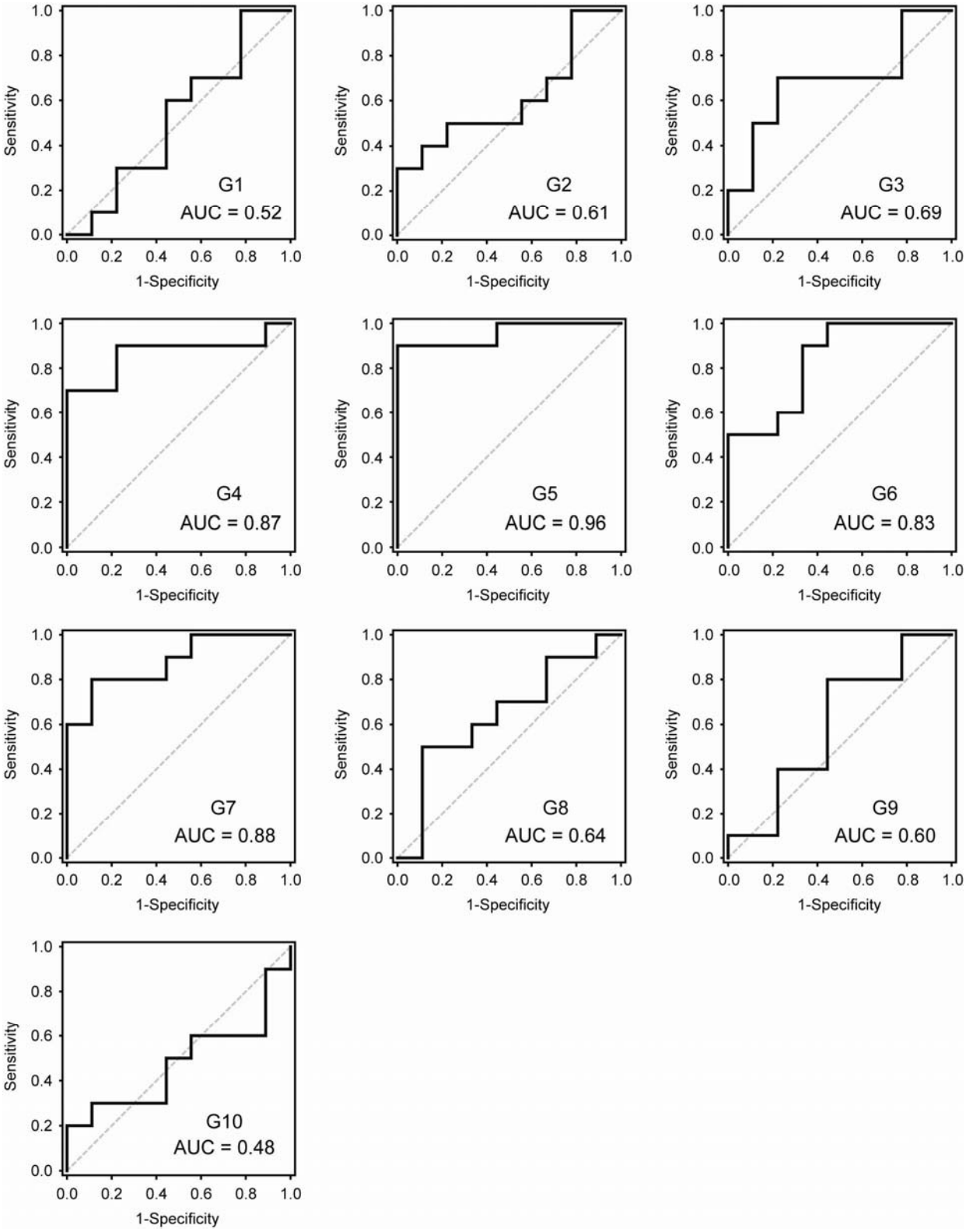

Supplementary Figure 11. ROC curves of fibrosing biomarkers.

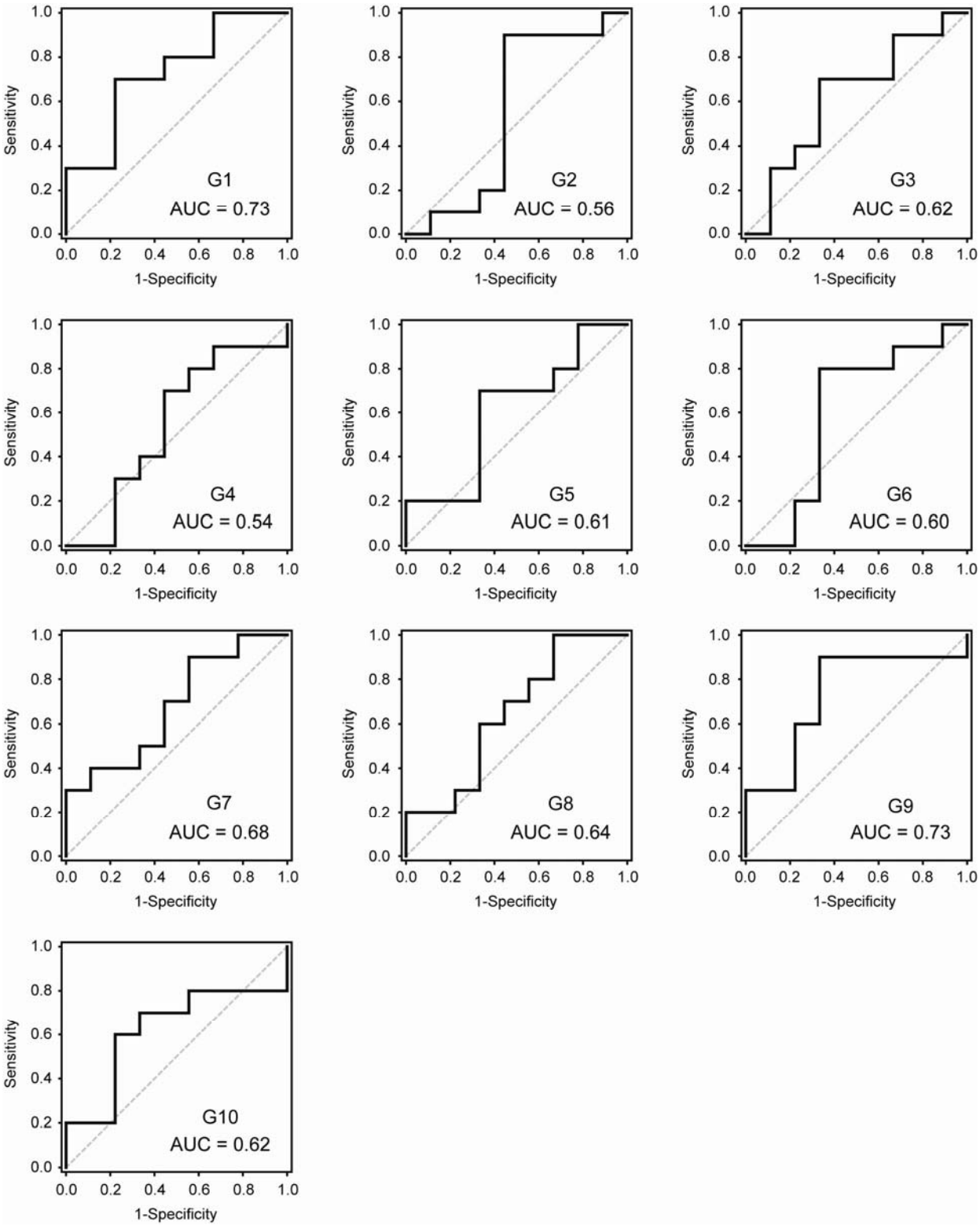

Supplementary Figure 12. ROC curves of resolving biomarkers.

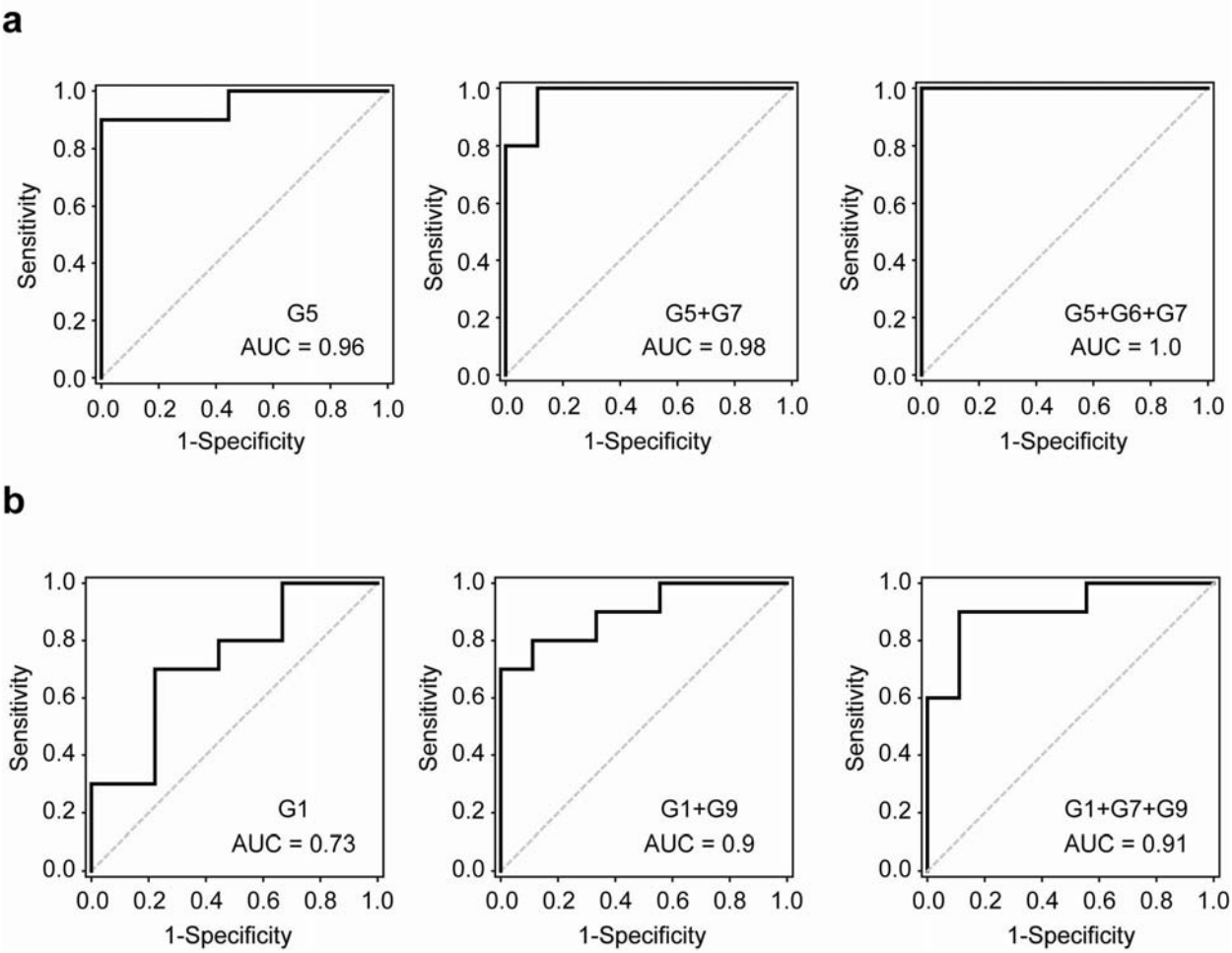

Supplementary Figure 13. Biomarker panels improve sensitivity and specificity. (**a**) ROC curves of the best single, dual and triple biomarker combinations of liver fibrosis with associated area under curves (AUC). (**b**) ROC curves of biomarkers associated with fibrotic resolution.

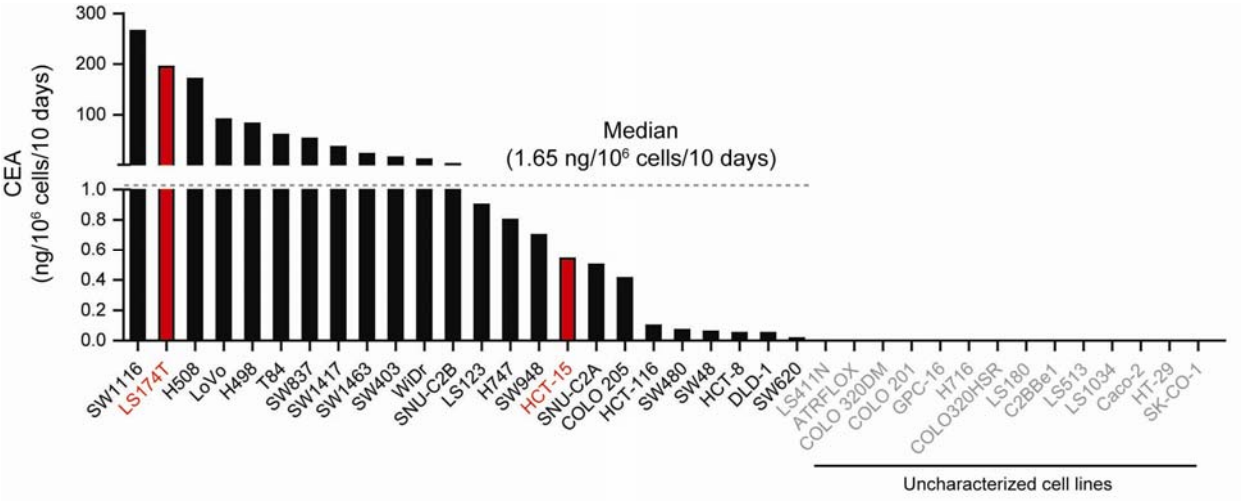

Supplementary Figure 14. Range of CEA secretion rates by established human colorectal cancer lines. Rates of 24 cell lines were collected from online documentation provided by ATCC; an additional 14 CRC lines were available but uncharacterized (grey). CEA secretion rates ranged well over 4 log units (15 pg–260 ng/10^6 cells/10 days). LS174T was 1 of 3 lines capable of producing CEA > 100 ng/10^6 cells/10 days, a rate > 300 fold higher than HCT-15 (0.54 ng/10^6 cells/10 days).

a

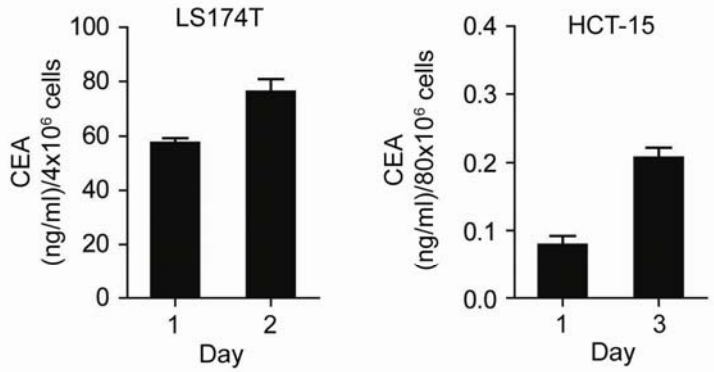

b

Standard (ng/ml)	Replicate 1 (A450)	Replicate 2 (A450)	Average	STD (x10^{-2})	CoV (%)
6.25	0.82	0.85	0.8474	1.84	2.20
3.13	0.50	0.49	0.49	0.90	1.82
1.56	0.30	0.30	0.30	0.24	0.81
0.78	0.20	0.19	0.20	0.38	1.96
0.39	0.13	0.14	0.14	0.97	7.10
0.20	0.12	0.11	0.11	0.38	3.37
PBS	0.08	0.082	0.081	0.17	2.10

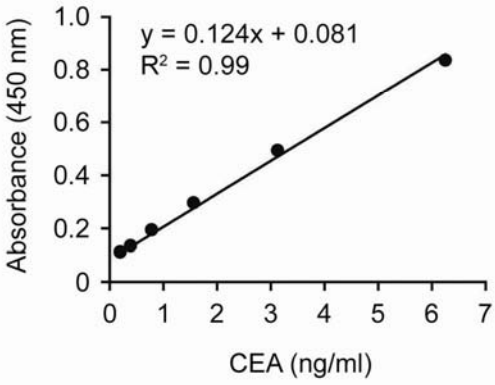

Supplementary Figure 15. *In vitro* CEA secretion by LS174T and HCT-15 colorectal cancer cells. (**a**) Quantification of CEA from conditioned media by ELISA. (**b**) Details of ELISA assay from Calbiotech. Standards were further diluted to enable quantification of CEA at low levels with a limit of detection of ~ 0.1 ng/ml.

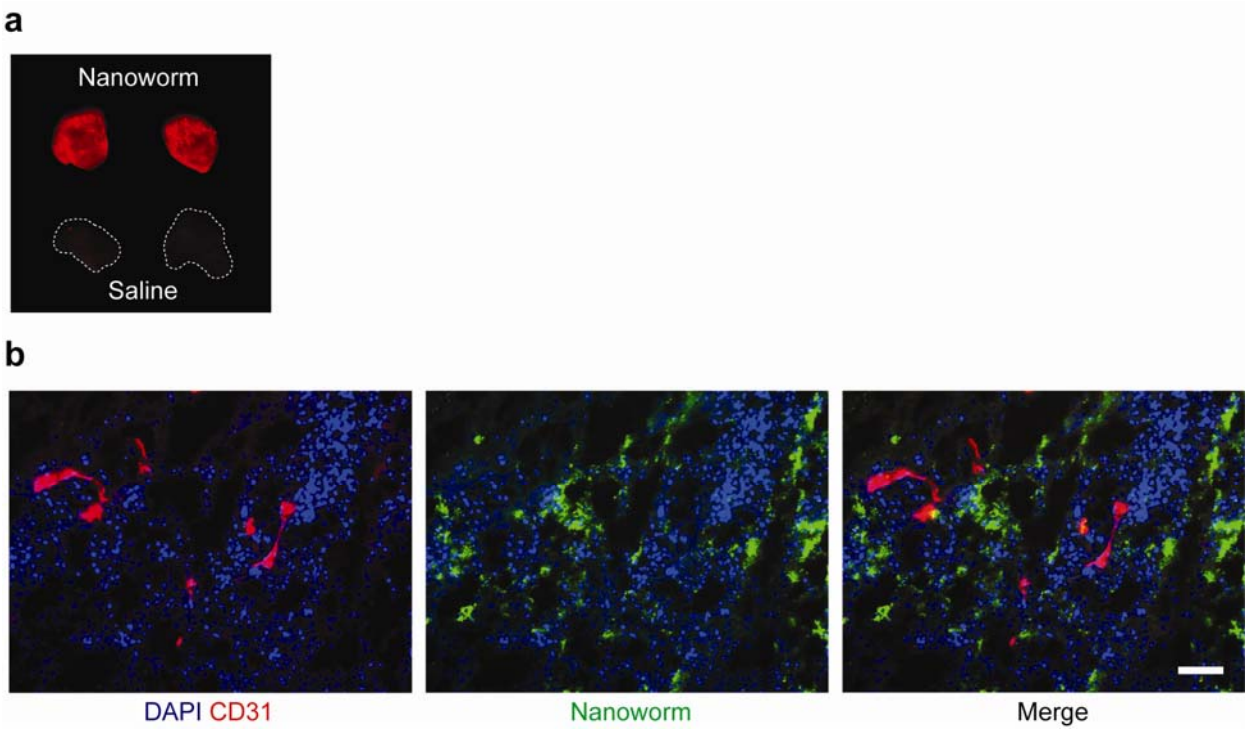

Supplementary Figure 16. NW accumulation in tumor tissue. (**a**) VivoTag-680-labeled NWs or saline solutions were injected into LS 174T xenograft animals. Following excision, the tumors were scanned for NW accumulation. (**b**) Immunofluoresence analysis of tumor sections for blood vessels (red) and NW (green). Scale bar = 50 μm.

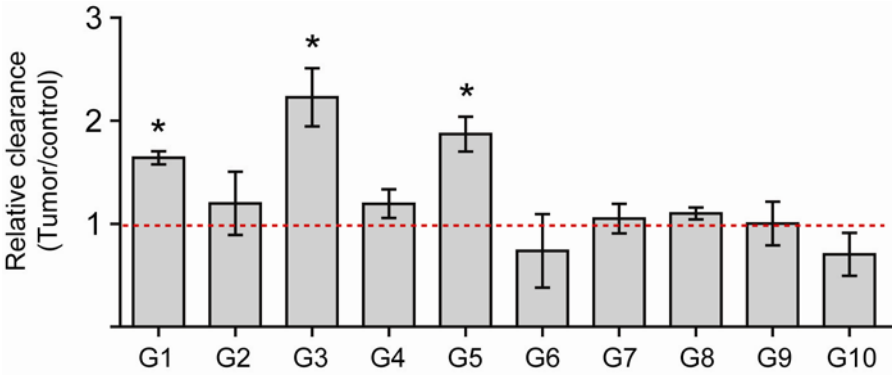

Supplementary Figure 17. 10-plex LS174T tumor signature. Biomarker clearance from LS174T tumor-bearing animals over control (* $P < 0.05$, error bars = s.d.).

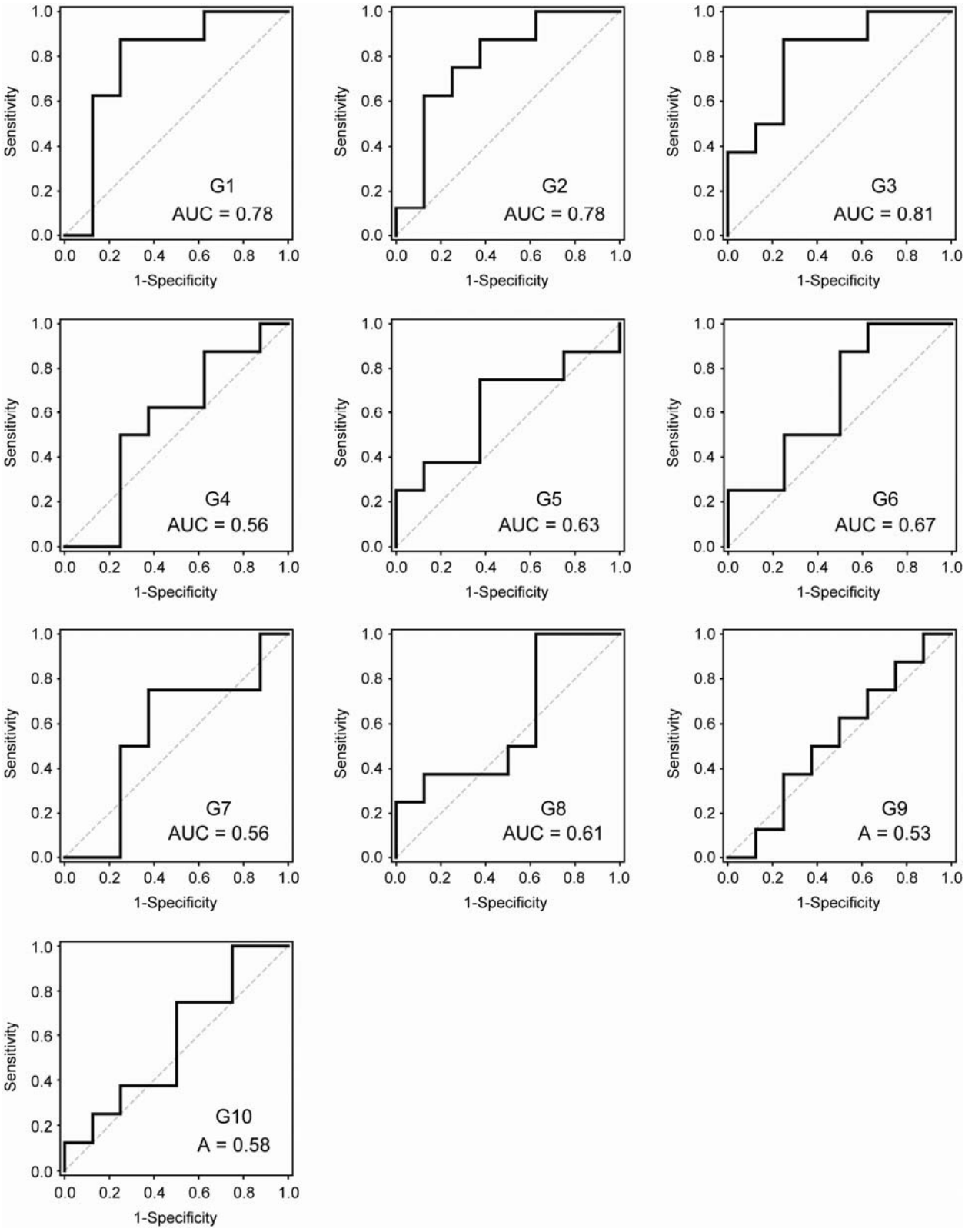

Supplementary Figure 18. ROC curves of tumor biomarkers.

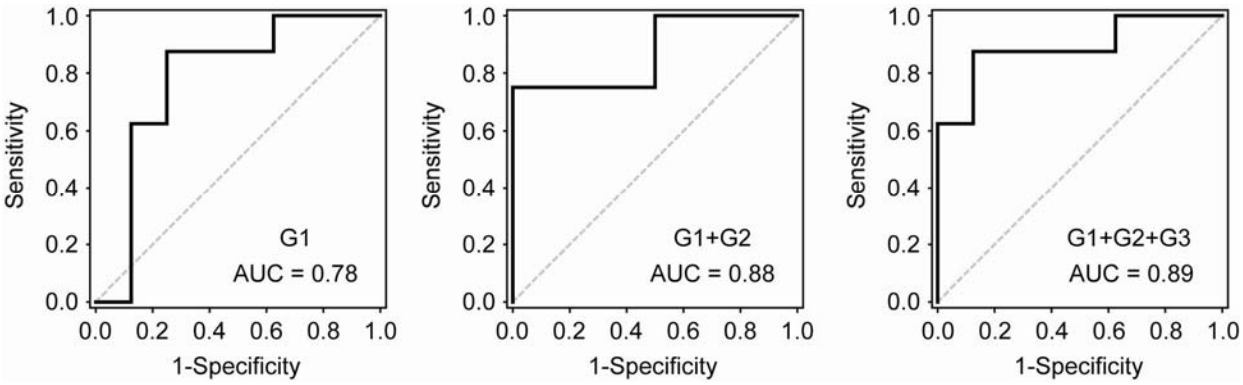

Supplementary Figure 19. Biomarker panels increase detection sensitivity and specificity of LS174T tumors. The collective area-under-curves (AUC) of the best single (G1, blue), double (G1+G2, green) and triple (G1+G2+G3, red) biomarker combinations.